Journal of Non-Newtonian Fluid Mechanics 171–172 (2012) 17–30

Contents lists available at SciVerse ScienceDirect

Journal of Non-Newtonian Fluid Mechanics

journal homepage: http://www.elsevier.com/locate/jnnfm

On creeping flow of a Bingham plastic fluid past a square cylinder

N. Nirmalkar [a], R.P. Chhabra [a,*], R.J. Poole [b]

[a] Department of Chemical Engineering, Indian Institute of Technology, Kanpur 208 016, India
[b] School of Engineering, University of Liverpool, Liverpool L69 3GH, United Kingdom

ARTICLE INFO

Article history:
Received 23 August 2011
Received in revised form 15 December 2011
Accepted 24 December 2011
Available online 12 January 2012

Keywords:
Square cylinder
Bingham number
Drag
Yield surface
Unyielded zone

ABSTRACT

In this work, the *2-D* creeping flow of Bingham plastic fluids past a cylinder of square cross-section has been studied numerically. The governing differential equations (continuity and momentum) have been solved over a wide range of Bingham number as $1 \leqslant Bn \leqslant 10^5$. Similar to the case of a circular cylinder, three zones of unyielded regions are seen to be present in the vicinity of the submerged cylinder, namely, caps attached to the top and bottom surfaces of the square cylinder, two sectors situated on the lateral sides undergoing rigid-body like motion and the usual far away unyielded regions. The influence of the Bingham number on their size and on the stress (normal and shear components) field in the vicinity of the cylinder is discussed in detail. In addition, the corresponding rate of strain, pressure and stress contours are also presented to facilitate the visualization of the structure of the flow field for scores of values of Bingham number. Also, the present numerical drag results have been correlated with the Bingham number via a simple expression thereby enabling their interpolation for the intermediate values of Bingham numbers.

1. Introduction

Many structured substances encountered in wide-ranging industrial settlings exhibit the so-called viscoplastic behaviour [1–4]. Typical examples include foams, filled polymer melts and solutions, clay and mineral suspensions and certain polymer solutions [1,2]. This class of materials is characterized by the existence of a threshold stress level (known as yield stress) below which the fluid does not shear and deforms like an elastic solid. Once the applied stress exceeds the yield stress, such a fluid may exhibit a constant shear viscosity (Bingham plastic fluid) or a shear-thinning viscosity (often approximated by the familiar Herschel–Bulkley fluid model) [3,4]. Whether a true yield stress exists or not, the flow behaviour of many complex materials can be well approximated by postulating the presence of a yield stress. Owing to the wide occurrence of such fluids in the processing and/or manufacturing of food stuffs, personal-care and pharmaceutical products, drilling muds, and cleaning fluids, significant research effort has been expended in elucidating the influence of yield stress on momentum and heat transfer characteristics for such fluids in circular and non-circular ducts, and mixing vessels. [3,4]. Owing to the presence of yield stress, parts of the flow domain are characterized by the so-called yielded or fluid-like regions (whenever the prevailing stress levels are higher than the yield stress) and unyielded or solid-like regions where the stress level is below the yield stress.

In contrast, the analogous studies on external flows like that over objects of different shapes are much more limited. From a theoretical stand point, the constitutive equations for visco-plastic fluids have discontinuity inherent in them which makes the delineation of the boundaries separating the yielded and unyielded regions rather difficult, in both numerical treatments and experimental studies. An inspection of the available literature on this subject [4] reveals that a bulk of the theoretical, numerical and experimental studies is concerned with the flow past a sphere [5–15]. While in some of the experimental studies [5–7,15], the objective has been to establish the dependence of drag coefficient on the pertinent dimensionless groups like Bingham number, Oldroyd number, and power-law index, for freely falling spheres in model test fluids with yield stress in unconfined and confined media. While some authors [10] have attempted to evaluate the yield stress of the fluid from the measurement of force–velocity data by extrapolating them to zero velocity. Yet others [11] have examined the combined effects of thixotropy and yield stress on the sedimentation velocity of a sphere in a stationary medium. The first numerical study for the creeping flow of a Bingham plastic fluid past an unconfined sphere is due to Beris et al. [12]. They used the free-boundary formulation together with a finite element/Newton method. Not only they provide detailed results on the flow, stress field and drag coefficient, they also put forward a dimensionless criterion for ascertaining whether a sphere (of known size and density) will settle under its own weight in a

* Corresponding author. Tel.: +91 512 2597393; fax: +91 512 2590104.
E-mail address: chhabra@iitk.ac.in (R.P. Chhabra).

0377-0257/$ - see front matter © 2012 Elsevier B.V. All rights reserved.
doi:10.1016/j.jnnfm.2011.12.005

Nomenclature

Bn	Bingham number ($\equiv\tau_0 d/\mu_B V$), dimensionless
C_D	drag coefficient, dimensionless
C_{DP}	pressure drag coefficient, dimensionless
d	side length of square cylinder, m
F_D	drag force per unit length of cylinder, N m^{-1}
F_{DP}	pressure drag force per unit length of cylinder, N m^{-1}
L	side of the square domain, m
m	growth rate parameter, s
p	pressure, Pa
$\boldsymbol{V}$	velocity vector, m s^{-1}
V	average velocity, m s^{-1}
V_x	velocity component in x-direction, m s^{-1}
V_y	velocity component in y-direction, m s^{-1}
x,y	Cartesian co-ordinates, m
Greek symbols	
δ	viscoplastic boundary layer thickness, m
∇	Del operator, m^{-1}
η	apparent viscosity, Pa s
ϕ	obtuse angle in static zone, Zr2, °
$\dot{\gamma}$	rate of strain tensor, s^{-1}
μ_B	plastic viscosity, Pa s
τ	extra stress tensor, Pa
τ_0	yield stress, Pa
θ	Meridian angle around circular cylinder, °

viscoplastic medium of known density and yield stress. Subsequently, Mitsoulis and co-workers [13,14] have extended this work for the flow of Bingham and Herschel–Bulkley fluid models over a sphere in cylindrical tubes to ascertain the extent of wall effects. They used the so-called fixed-domain approach. However, both the free-boundary and fixed domain yield nearly identical values, as noted by Liu et al. [16]. In the preceding numerical studies [13,14], the discontinuity in the constitutive equations for viscoplastic materials was treated via the so-called regularization method due to Papanastasiou [17]. Broadly, there is a fair degree of match between the experimental and predicted values of the yielded regions and drag coefficient for a sphere settling in Bingham and Herschel–Bulkley model fluids [4].

Similarly, a few studies are also available on the *2-D* creeping flow past a circular cylinder. The earliest results for an unconfined circular cylinder are due to Adachi and Yoshioka [18] who obtained approximate upper and lower bounds on drag coefficient by employing the velocity and stress variational principles. The trial velocity and stress functions used by them [18] lead to the existence of elliptical fluid-like zones surrounding the cylinder without any appeal to the fact that whether or not it was a yield surface. In spite of this limitation, together with the approximate nature of their analysis, they concluded that the lower bound predictions of drag were reliable for $Bn \leqslant 100$ whereas the purely plastic predictions based on the slip-line analysis were adequate for $Bn > 100$. These inferences are however based on intuitive and heuristic considerations without any sound justification. The first full numerical study of the creeping flow of Bingham plastic fluids past a cylinder confined symmetrically between two plane walls is due to Roquet and Saramito [19]. They employed an anisotropic auto-adaptive mesh procedure together with the augmentation Lagrangian based finite element scheme. For the first time, they identified three unyielded zones particularly the so-called polar caps and islands for a range of values of the blockage ratio (height of the channel/diameter of cylinder) in the range 1.25–2, albeit a great majority of their results corresponds to the blockage ratio of 2. Subsequently, a similar study was reported by Mitsoulis [20] who varied the blockage ratio from 2 to 50, the latter value was regarded to be adequate to approximate the limiting case of the unconfined flow condition. By analogy with the wall effects on a sphere, the wall effects were found to be significant at low Bingham numbers. This is simply due to the fact that the yielded or fluid-like regions progressively diminish with the increasing value of the Bingham number and thus, it is likely that the fluid has already solidified before reaching the physical wall and therefore, no wall effect is expected under such conditions. Over the range $0.01 \leqslant Bn \leqslant 1000$, Mitsoulis [20] has reported the effect of Bingham number on the size of various unyielded regions around the cylinder. He also developed drag relationships based on his numerical predictions. Similarly, a recent study has also been reported by Tokpavi et al. [21] who used the Bingham constitutive equation with the Papanastasiou's regularization and reported the drag coefficient (C_D) and flow kinematics as a function of the Oldroyd number which is similar to the Bingham number. A viscoplastic boundary layer was also identified in the limit of plastic flow (*i.e.,* high Oldroyd number limit) and the viscoplastic boundary layer thickness was expressed as a function of the Oldroyd number. A detailed study on the shapes and location of the rigid zones was also reported. They supplemented their numerical predictions by employing the perfectly plastic analysis valid at high Bingham numbers ($Bn \to \infty$). The two drag predictions were in almost perfect agreement. The creeping flow past an unconfined circular cylinder in a Herschel–Bulkley viscoplastic fluid medium was investigated by Besses et al. [22] and the location of rigid zones, kinematics of the flow and drag coefficient were examined as a function of the shear-thinning index and the Oldroyd number (Od). Their results show that the size of rigid (unyielded) zones increases as the degree of shear-thinning increases or the power-law index is lowered. They also examined the role of partial slip on the surface of the cylinder and found that the slippage can reduce the hydrodynamic drag on the cylinder by about 33% with reference to its value for the no-slip condition. Zisis and Mitsoulis [23] explored the effect of blockage on the Poiseuille flow past a circular cylinder in a plane channel and proposed a correlation for the drag coefficient in terms of the blockage ratio and Bingham number. In contrast to the aforementioned studies in the creeping flow regime ($Re = 0$), Mossaz et al. [24] have recently examined the role of inertial forces (finite value of Reynolds number) on the onset of flow separation and of vortex shedding from a circular cylinder submerged in viscoplastic fluids. Indeed, both these phenomena (flow separation and vortex-shedding) differ significantly in this case from that in Newtonian and power-law fluids. Broadly, the yield stress of the fluid acts to stabilize the flow and vortex shedding is thus deferred to higher Reynolds numbers than that in Newtonian fluid and power-law fluids [25].

Recently, Putz and Frigaard [26] have not only critically reviewed the pertinent literature on this subject, but have also obtained new results for an elliptical cylinder confined between two plane walls via the use of weak formulations in terms of the resistance and mobility problems. Most of the aforementioned studies have employed the exponential regularization schemes of Papanastasiou [17], a few authors have also examined the merits and de-merits of this approach [16,27]. Liu et al. [16] compared the performance of the two regularization schemes, namely Papanastasiou [17] and Bercovier and Engelman [28] which was employed in [12], as applied to the creeping flow of Bingham model

fluids past a sphere. They concluded that while the drag predictions obtained with these two schemes are in good agreement, it is not possible to identify the apparently unyielded regions simply by using large values of the regularization parameter. Similarly, Frigaard and Nouar [27] evaluated the performance of different regularization schemes and concluded that regularization methods would result in maximum errors in lubrication-type flows as well as the viscosity regularization approach can lead to unrealistic predictions about the stability of flow.

In addition to the aforementioned studies pertaining to the flow past single spheres and cylinders, there have been a few experimental and numerical studies on hydrodynamic interactions between two spheres [9,29] and two cylinders [30,31]. Finally, before leaving this section, two more categories of studies need to be mentioned here, for these are also pertinent in the present context. Firstly, Oldroyd [32] developed a theoretical framework to analyze the boundary layer flow of Bingham plastic fluids past a plane surface at low Reynolds numbers. In the limit of large Bingham number and sufficiently small Reynolds number, by neglecting the acceleration terms, he was able to obtain an analytical solution to the approximate boundary layer equations for the flow past a plate. Broadly, the inclusion of normal stress term leads to the boundary layer thickness to vary along the surface as $\delta \sim x^{2/3}$ rather than the familiar $\delta \sim x^{1/2}$ variation seen for Newtonian fluids. Piau [33] has revisited the analysis of Oldroyd [32] by obtaining a similarity solution. Secondly, intuitively it appears that in the limit of $Bn \to \infty$, the shearing motion of the fluid ceases and therefore the hydrodynamic forces acting on structures of different shapes can be evaluated by assuming the perfectly plastic flow. This approach has been shown to yield reliable predictions for circular cylinders at large values of Bingham number by using the plasticity/slip-line analysis [34], albeit this approach does not entail the use of fluid characteristics at large Bingham numbers. On the other hand, behaviour in the limit of $Bn \to \infty$ has been treated well in Ref. [21] as far as the prediction of the drag force on a cylinder is concerned. Aside from spheres and cylinders, some experimental results are also available on drag forces for square cross-sections in soils [35], flat plates [37] and non-spherical particles in visco-plastic polymer solutions which have been thoroughly reviewed in Ref. [4]. Similarly, as noted earlier, numerical predictions for elliptical cross-section cylinders have been reported in [26]. Also, Knappett et al. [35] estimated the ultimate load on the cylinders of square and circular cross-sections using a wedge based upper-bound plasticity analysis and their predictions are in line with their own experiments carried out in a modified shear box. It is generally believed that such analyses are good under the conditions when no-slip condition is applicable [36]. It is also worthwhile to make another observation here. In the case of the circular cylinder, the slip-line analysis based on the perfectly plastic regime and the yield-surfaces revealed by numerical simulations at high Bingham numbers are very similar and close to each other and therefore the two drag predictions are in almost perfect agreement.

From the foregoing discussion, it is abundantly clear that with the notable exceptions of spheres and cylinders, no numerical results are available on the creeping flow of viscoplastic fluids past two-dimensional bodies of other shapes. This work endeavours to extend the currently available body of knowledge by studying the creeping flow of a Bingham plastic fluid past a *2-D* cylinder of square cross-section. The hydrodynamic forces exerted on support structures of rectangular cross-sections are relevant in marine and estuary flow applications. In the continuous thermal treatment of foodstuffs, food particles like sliced carrots and potatoes, etc. may be approximated like square bars and these are processed in xanthan gum and other polymer solutions which can exhibit visco-plastic behaviour under appropriate conditions. Apart from these potential pragmatic applications, there is a considerable theoretical interest in understanding the flow behaviour of yield stress fluids in geometries with sharp corners, e.g. see [38–41]. For instance, Atkinson and El-Ali [38] concluded that the behaviour of a yield-stress fluid around a sharp corner is more like that of a Newtonian fluid. This is so presumably due to the high shear rates which make the magnitude of the yield stress negligibly small as compared to the corresponding flow stress, *i.e.*, $|\mu_B \dot{\gamma}| \gg |\tau_0|$. Therefore, the visco-plastic flow past a square cylinder might also shed some light on this aspect of the bluff body flows. In particular, the governing differential equations are solved numerically together with the Bingham fluid model within the framework of Papanastasiou [17]. Extensive results on the location and size of unyielded regions, stress field and drag coefficient are presented over the range of Bingham number $1 \leqslant Bn \leqslant 10^5$.

2. Problem formulation

Consider an unconfined square cylinder of side, *d*, past which a Bingham plastic fluid is flowing slowly so that the inertial forces are negligible. To approximate the truly unconfined flow condition, the approach we adopt here is to assume an artificial domain (of square shape) with stress-free boundary walls. The length of the domain is $2L/d$ and the square cylinder is situated at its centre. Under the creeping flow assumption, this problem can be solved using two axes of symmetry and hence one needs to solve the governing differential equations over only one quarter of the computational domain as shown in Fig. 1. Since the cylinder is infinitely long in the *z*-direction, there is no flow in *z*-direction and no flow variable depends upon *z*, *i.e.* $V_z = 0$ and $\frac{\partial()}{\partial z} = 0$. Thus, the flow is two-dimensional. For the incompressible, steady and creeping flow, the equations of motion can be written as follows:

$$\nabla \cdot \boldsymbol{V} = \boldsymbol{0} \tag{1}$$

$$-\nabla p + \nabla \cdot \tau = 0 \tag{2}$$

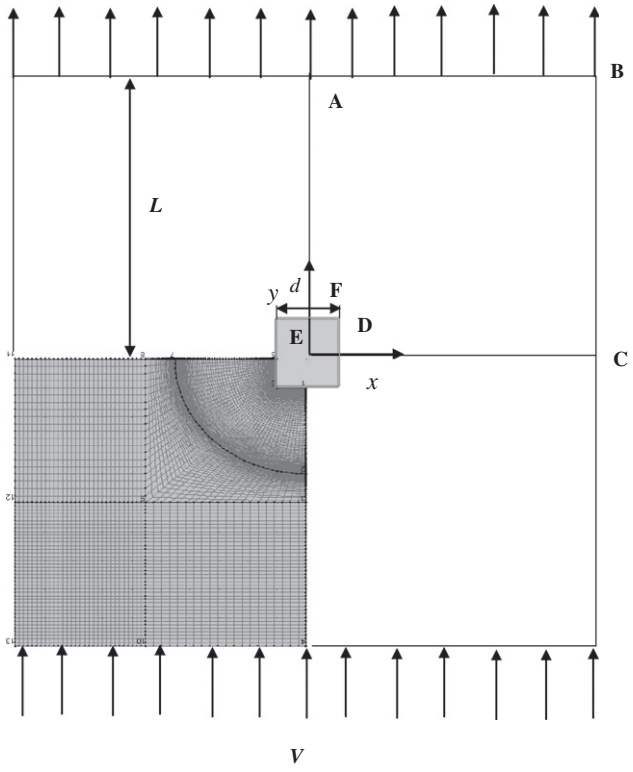

Fig. 1. Schematic diagram of flow domain.

The deviatoric part of the stress tenser τ is given by the Bingham plastic constitutive relation [1] which for a simple shear flow can be written as follows:

$$\tau = \tau_0 + \mu_B\dot{\gamma} \quad \text{if } |\tau| > |\tau_0| \tag{3}$$

$$\dot{\gamma} = 0 \quad \text{if } |\tau| \leqslant |\tau_0| \tag{4}$$

Unfortunately, owing to its discontinuous nature, it is very difficult to solve numerically the field equations together with Eq. (3). In order to overcome this difficulty, Papanastasiou [17] proposed a modified model with a growth rate parameter (m) which provides not only a smooth transition from no-flow region to flow region, but also leads to better convergence and accurate prediction of the size and shape of rigid zones. Hence by using the Papanastasiou modification, the Bingham plastic model can be re-written as follows:

$$\tau = \tau_0[1 - \exp(-m\dot{\gamma})] + \mu_B\dot{\gamma} \tag{5}$$

It is clear from Eq. (5) that with high values of the growth rate parameter, m, the model tends towards the original Bingham plastic model but at the same time at very high values of the growth rate parameter, numerical problems begins to emerge. In addition, as noted in previous studies [27], this model represents the solid region by a fluid of very high viscosity. The location of the rigid zones within the flow region also depends on the value of the growth rate parameter and therefore it is necessary to establish the influence of this parameter on the numerical results. Mitsoulis [20] examined the effect of the regularization parameter on the drag coefficient for a circular cylinder and found that a value of $m = 10^3$ s was sufficient. On the other hand, for the results to be free from such numerical artifacts, Tokpavi et al. [21] used $m = 10^4$ s and $m = 10^5$ s for low and high plasticity effects respectively. Evidently, a prudent choice of the value of m is vital for the results to be free from such numerical artifacts.

For incompressible fluids, the deviatoric stress tensor can be written as follows:

$$\tau = 2\eta\dot{\gamma} \tag{6}$$

and the scalar viscosity η is given by:

$$\eta = \mu_B + \frac{\tau_0}{|\dot{\gamma}|}[1 - \exp(-m|\dot{\gamma}|)] \tag{7}$$

where $\dot{\gamma}$ is rate-of-strain tensor which is given by

$$\dot{\gamma} = \frac{1}{2}(\nabla V + \nabla V^T) \tag{8}$$

The magnitude of rate of deformation tensor and deviatoric stress tensor is given by

$$|\dot{\gamma}| = \sqrt{\frac{1}{2}tr(\dot{\gamma}^2)} \tag{9}$$

$$|\tau| = \sqrt{\frac{1}{2}tr(\tau^2)} \tag{10}$$

In the limit of creeping flow, this problem is governed by the single dimensionless group called the Bingham number which is the ratio of the yield stress to viscous stress and can be written in the following manner:

$$Bn = \frac{\tau_0 d}{\mu_B V} \tag{11}$$

Note that this definition of Bingham number differs by a factor of two from the Oldroyd number used in [21]. The variables appearing in the governing equations and boundary conditions are rendered dimensionless using d, V and τ_0 as scaling variables for length, velocity and stress components respectively.

As noted earlier, this problem can be considered with two planes of symmetry; hence one quarter of the domain is used to reduce the required computational efforts (see Fig. 1). In light of these symmetry planes, the following boundary conditions are used in this work:

- Along the y-axis symmetry (line AF in Fig. 1)

$$V_x = 0 \quad \text{and} \quad \frac{\partial V_y}{\partial x} = 0 \tag{12}$$

- Along the x-axis symmetry (CD)

$$V_x = 0 \quad \text{and} \quad \frac{\partial V_y}{\partial y} = 0 \tag{13}$$

- On the surface of the cylinder: no-slip condition is prescribed, i.e.,

$$V_x = 0 \quad \text{and} \quad V_y = 0 \tag{14}$$

- On the boundaries (AB) and (BC)

$$V_x = 0 \quad \text{and} \quad V_y = V \tag{15}$$

- The pressure point constrained boundary condition is used at point C and a zero value of pressure is prescribed at this point.

The drag coefficient is the measure of the total force exerted by the fluid on the cylinder in the direction of flow and it is defined here as:

$$C_D = \frac{F_D}{\tau_0 d} \tag{16}$$

And the pressure component of the drag coefficient, C_{DP}, can be expressed as follows:

$$C_{DP} = \frac{F_{DP}}{\tau_0 d} \tag{17}$$

The scaling considerations suggest both C_D and C_{DP} to be functions of the Bingham number only. This work endeavours to explore and develop this functional relationship for a square cylinder.

3. Numerical solution methodology

The governing differential equations subject to the aforementioned boundary conditions have been solved numerically using the finite element based solver COMSOL Multiphysics (Version 4.0) for both meshing the computational domain as well as to map the flow domain in terms of the primitive variables u–v–p. Since gradients are expected to be steep near the cylinder surface as well as near the interface between the rigid (unyielded) and fluid (yielded) zones, a fine mesh is required in both these regions. In this study, quadrilateral cells with non-uniform spacing have been used to mesh these regions of the computational domain. Furthermore, the steady, *2-D*, creeping flow module is used with PARDISO scheme to solve the system of equations. The Bingham plastic model with Papanastaiou regularization [17] was used for approximating the extra stress tensor in the momentum equation. A user defined function (UDF) has been introduced for this purpose and to estimate the value of absolute viscosity. The solution was always initiated using the converged Newtonian flow field. A relative convergence criterion of 10^{-5} for the equations of continuity and momentum were used and further reduction in the tolerance level had a negligible effect on the results (less than 0.01% in C_D and C_{DP}, for example).

4. Choice of numerical parameters

Evidently, the accuracy and reliability of the numerical solution depends on an appropriate choice of domain and grid characteristics. In the present context, the domain is characterized by a square

Table 1
Domain independence test at $Bn = 1$.

Domain size (L)	Elements	C_D	C_{DP}
2	3000	38.31	30.12
3	7500	37.19	29.65
5	10,600	34.32	29.12
7	12,500	33.43	22.41
10	17,900	33.43	22.31
15	18,547	33.43	22.31
20	19,654	33.43	22.31

Table 2
Grid independence test.

Grid	Elements	C_D		C_{DP}	
		$Bn = 1$	$Bn = 1 \times 10^5$	$Bn = 1$	$Bn = 1 \times 10^5$
G1	9500	33.02	14.85	21.31	11.05
G2	14,500	33.21	14.89	21.62	11.67
G3	19,300	33.43	14.91	22.43	12.08
G4	25,200	33.43	14.92	22.45	12.09

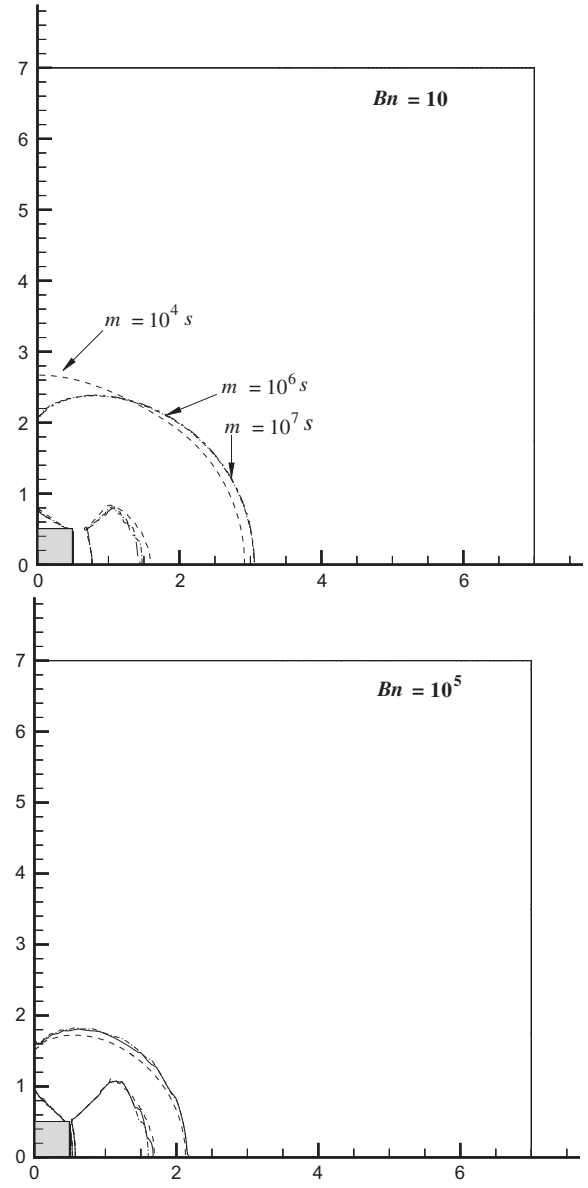

Fig. 2. Effect of regularization parameter, m on the location of yield surface at $Bn = 10$ and $Bn = 10^5$.

of side length L. In this work, the effect of the domain was studied by systematically varying the value of L/d as 2, 3, 5, 7 and 10. The resulting change in the values of the pressure and total drag coefficients is summarized in Table 1, where it is clearly seen that there is no significant change in the results when the domain size is increased from $L/d = 7$ to $L/d = 10$. On other the hand, the required CPU time increased several fold. Thus, $L/d = 7$ denotes an acceptable compromise between the accuracy of the results on one hand and the required computational effort on the other. Furthermore, in order to show the adequacy of the value of L/d used here, limited additional simulations were also performed using $L/d = 15$ and 20. The resulting values were found to be virtually indistinguishable from that obtained with $L/d = 7$. Next, we turn our attention to the selection of an optimum grid. Four non-uniform grids which were sufficiently fine close to the cylinder as well as to the interface between the solid and fluid zones for accurate prediction of the yield surface were investigated. The effect of the grid characteristics on the value of the pressure and total drag coefficients is shown in Table 2 for the extreme value of the Bingham number. Once again, grid G3 is seen to be satisfactory, for there is a negligible change in the results obtained with G3 and G4. Initially, the approximate location of yield surfaces was identified using a relatively coarse mesh and the numerical resolution in this region was progressively improved by systematically refining the mesh. Thus, in a sense, a manual adaptive mesh was used to delineate the position of the yield surface with a degree of precision. Also, a mesh found suitable for maximum value of the Bingham number is likely to be satisfactory for lower values of the Bingham number.

As noted earlier, the location of the rigid zones strongly depends upon the value of the regularization parameter, m. A low value of m may lead to an incorrect prediction of the location of the yield surface [12]. On the other hand, very high values may result in

Table 3
Drag on a square cylinder in Newtonian fluids at $Re = 1$.

Authors	Drag coefficient C_D
Sharma and Eswaran [42]	14.416
Dhiman et al. [43]	14.330
Present	14.521 (COMSOL) 14.440 (FLUENT)

Table 4
Drag on a circular cylinder in Bingham plastic fluid ($Re = 0$).

Bn	Drag coefficient C_D		
	Tokpavi et al. [21]	Zisis and Mitsoulis [23]	Present
1	–	22.060	20.314(21.061)*
10	14.644	15.629	14.251(14.921)
1×10^2	12.536	12.592	12.421(12.520)
5×10^2	12.166	11.700	12.214(12.305)
1×10^3	12.096	11.700	11.987(11.981)
1×10^5	11.985	11.700	11.954 (11.921)

* Values in parenthesis are based on $m = 1000$ s.

Table 5
Drag coefficient in the limit of infinite plasticity for a circular cylinder.

References	C_D^∞
Randolph and Houlsby [34]	11.940
Adachi and Yoshioka [18]	10.280
Tokpavi et al. [21]	11.940
Present	11.954

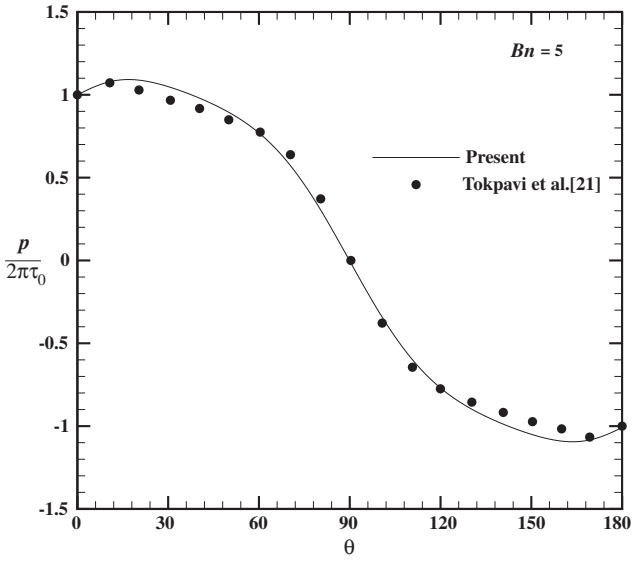

Fig. 3. Comparison of non-dimensional surface pressure with Tokpavi et al. [21] for a circular cylinder ($\theta = 0$ denotes the front stagnation point).

numerical oscillations in the solution and it generally leads to poor convergence [16]. Most of the previous studies have used $m = 10^3$ s [13,14]. An extensive study has been performed by Tokpavi et al. [21] on this aspect who classified the flow into two regimes depending upon the value of the Bingham number, low plasticity (small values of *Bn*) and high plasticity (large values of *Bn*) respectively. They used $m = 10^4$ s for the so-called low plasticity flow and $m = 10^5$ s for the high plasticity effects. Additional exploration was carried out in the present study. Fig. 2 shows the effect of the value of m on the shape of the yield stress. It is clearly seen that the results are virtually indistinguishable from each other for $m \geqslant 10^6$ s at both values of the Bingham number. Based on these observations, we have used $m = 10^6$ s for all simulations reported herein. However, strictly speaking, this method of choosing an appropriate value of m is a matter of trial and error. On the other hand, in an envisaged application if one were able to identify two independent scales to normalize the velocity and strain rate, one can then develop a systematic strategy to choose the value of m to deal with the so-called small strain rates in an unambiguous manner.

5. Results and discussion

Extensive new results on the detailed kinematics of the creeping visco-plastic fluid flow ($Re = 0$) over a square cylinder have been obtained spanning five-orders of magnitude variation of the Bingham number. However, prior to undertaking the detailed presentation and discussion of the new results, it is instructive to demonstrate the reliability and precision of the solution methodology and of the choice of the numerical parameters used in this work. This objective is accomplished by way of presenting a few benchmark comparisons with the prior results available in the literature.

5.1. Validation of results

While no prior results are available for a square cylinder in Bingham plastic fluids except for that of Knappett et al. [35] in the fully plastic regime, reliable numerical results are now available for this configuration in Newtonian fluids [42,43] and for a circular cylinder [19–21] and a sphere [12] in Bingham plastic media.

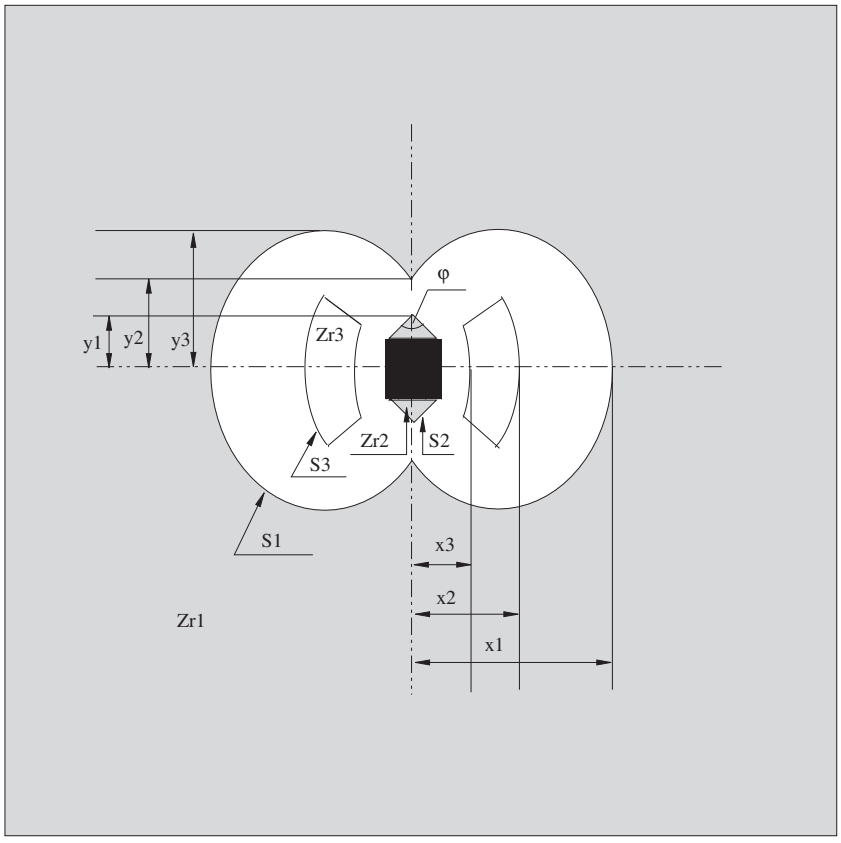

Fig. 4. Schematic representation of the characteristics of the rigid zones around a square cylinder (flow is in upward direction).

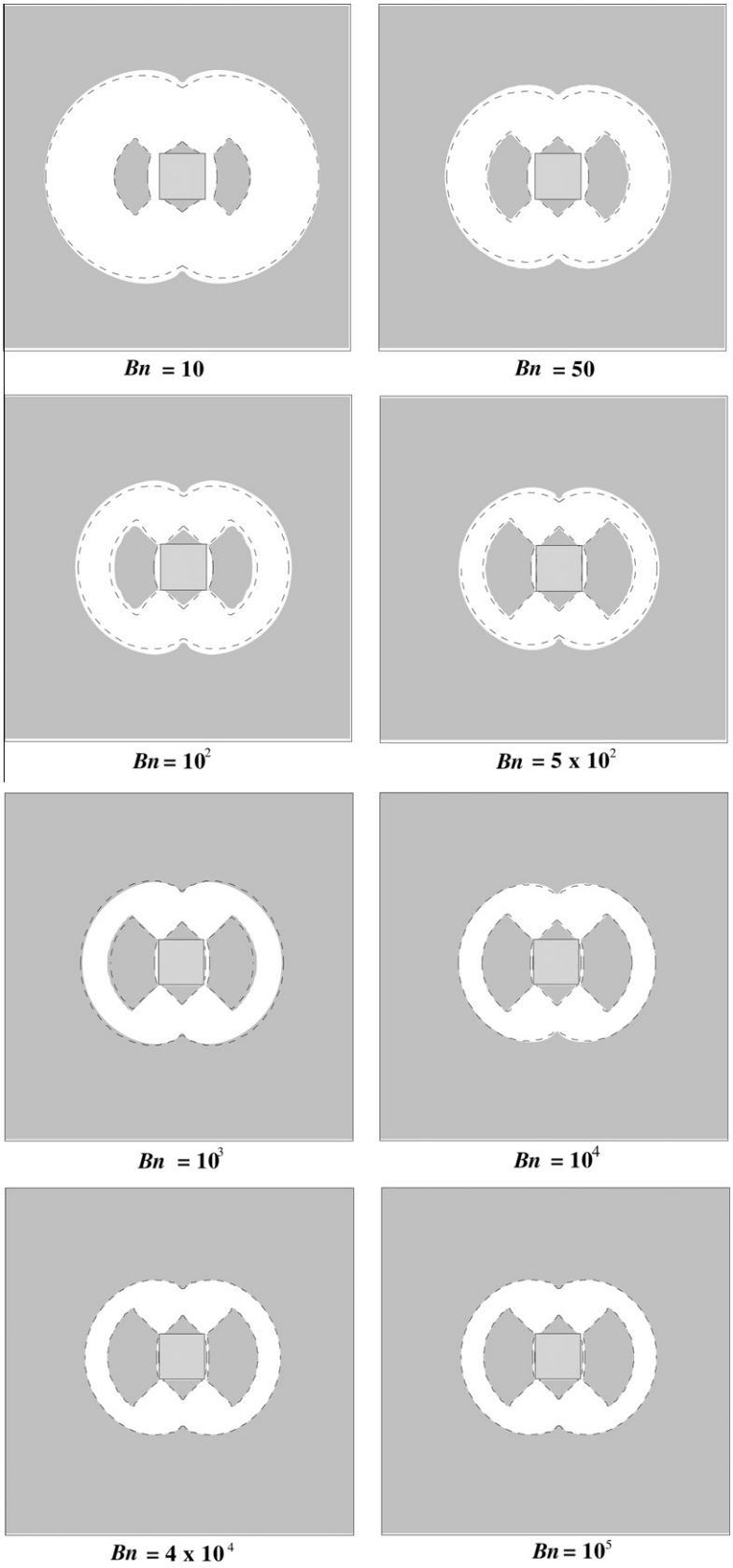

Fig. 5. Effect of Bingham number on the unyielded fluid zones (dashed line represents bi-viscosity model).

These are used here for validating the present solution methodology. Note that an in-house finite volume code with different domain and grid structure was used in Refs. [42,43]. Table 3 shows a comparison for a square cylinder in Newtonian fluids where an excellent match is seen to exist between the present and literature values of the drag coefficient at Reynolds number of unity. It is

appropriate to add here that the differences of this order are not at all uncommon in such numerical studies, e.g., see [44]. Next, Table 4 shows a similar comparison for the creeping flow of Bingham plastic fluids past a circular cylinder for a range of values of the Bingham number. While the present results are seen to be virtually indistinguishable from that of Tokpavi et al. [21], the present values differ by about 8–9% from that of Zisis and Mitsoulis [23], especially at low values of the Bingham number. While the exact reasons for such a large discrepancy are not immediately obvious, one possible explanation is the relatively small value of $m = 10^3$ s used in their study, To add further weight to this assertion, the results obtained with $m = 10^3$ s are also included in parentheses and clearly these values are seen to be closer to that of Zisis and Mitsoulis [23]. Finally, it needs to be emphasized here that the number of elements is much larger in the present case than that used in [23] and this may partly be responsible for these differences. Furthermore, as noted earlier, at very high values of the Bingham number, the flow can be assumed to be purely plastic in nature and in this limit, the present results are compared in Table 5 with that based on the plasticity theory [21,34], It is clearly seen here that the results deduced from the plasticity theory are in good agreement with the present results at high Bingham numbers for a circular cylinder. Such a close correspondence inspires confidence in the reliability of numerics used in this work.

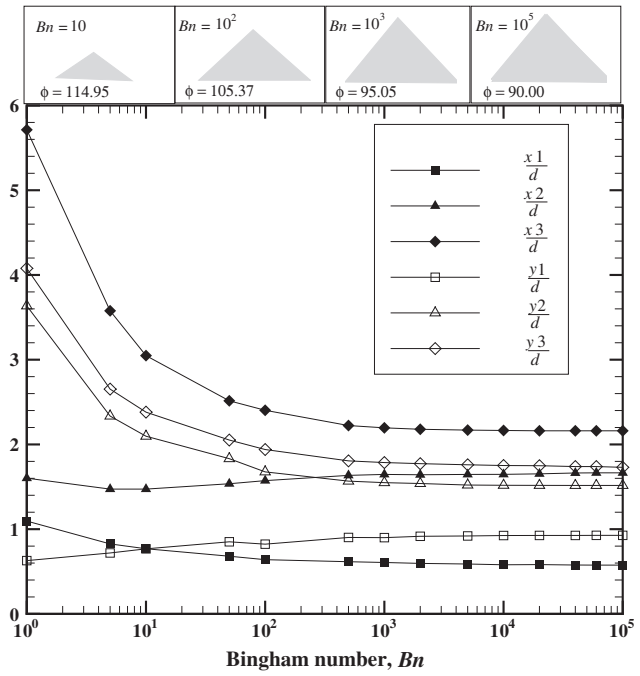

Fig. 6. Variation of the rigid zone in x-direction (solid symbols) and in y-direction (hollow symbols) together with variation of ϕ with Bingham number.

Table 6
Comparison of the size of rigid zones between a square and circular cylinder at $Bn = 20$.

	Circular cylinder [21]	Square cylinder
$\frac{x_1}{d}$	0.60	0.73
$\frac{x_2}{d}$	0.91	1.55
$\frac{x_3}{d}$	2.75	2.78
$\frac{y_1}{d}$	0.55	0.81
$\frac{y_2}{d}$	1.60	1.96
$\frac{y_3}{d}$	1.87	2.22

In addition to such overall comparisons, Fig. 3 shows a comparison in terms of the present prediction of pressure distribution on the surface of a circular cylinder with that of Tokpavi et al. [21] and once again, an excellent match is seen to exist. In our view, such a close correspondence between the surface pressure profiles provides a much more stringent testimony to the reliability of the present results than that seen in Tables 3–5. In view of the aforementioned comparisons, the new results reported herein for a square cylinder are believed to be reliable to within 1–2%.

5.2. Definition of rigid zones and fluid zones

The yield surface is the interface between the unyielded (solid-like) and yielded or fluid-like zones. In the case of the flow past a circular cylinder and sphere, the shape and location of the yield surface has been examined by several authors and we essentially follow a similar approach here to define the rigid zones. As in the

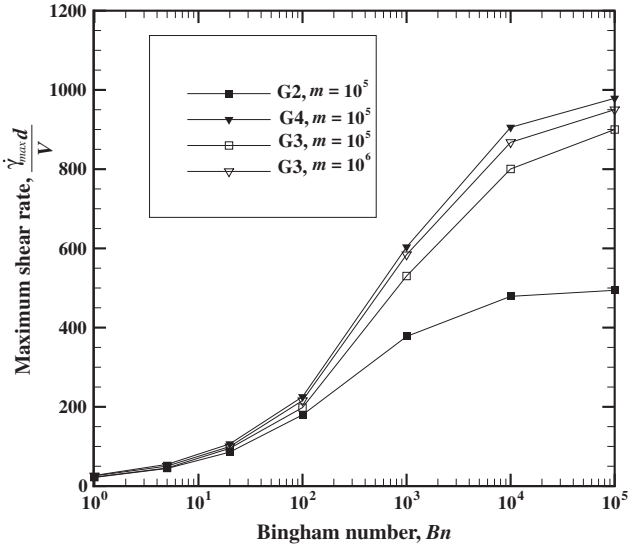

Fig. 7. Dependence of maximum shear rate along the surface of the cylinder on Bingham number.

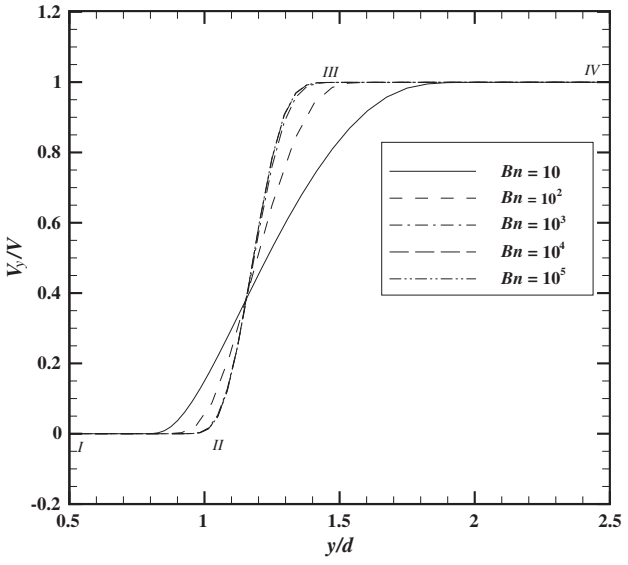

Fig. 8. Velocity profile along the line of symmetry ($x = 0$) in the y-direction.

case of a circular cylinder and a sphere, three distinct solid zones are observed in the present case also; however, they are different in shape in the case of a square cylinder studied here. A schematic of such regions together with their definitions is shown in Fig. 4.

- A far-field solid zone, Zr1, is characterized by the values of x_1 and y_3 and the corresponding yield surface is designated as S1 (Fig. 4). This zone is dynamic in that the material is moving as a solid plug with a uniform velocity V. The shape of S1 is qualitatively similar to that observed for a sphere [13].
- Two stagnant zones, Zr2, at the top and at the bottom of the cylinder are characterized by their height y_1 and the obtuse angle, ϕ. As in the case of circular cylinder and sphere, this zone is of triangular shape. The yield surface is denoted by S2. In the case of a circular cylinder, this zone is referred to as "*polar caps*". These zones are static and are attached to the cylinder [21].
- Two dynamic zones, Zr3, equidistant from the cylinder on the either side about the x-axis, are characterized by x_2 and x_3. In contrast to the other rigid zones, the shape of these zones is quite different from that observed in the case of circular cylinders and spheres. This zone is undergoing a rigid body-like rotation and the strength of rotation increases with the increasing value of the Bingham number. This yield surface is denoted by S3 which also moves with a constant velocity V. In the case of a circular cylinder, these zones are referred to as "*islands*" [21].

Naturally, the size of the aforementioned boundaries demarcating the unyielded and yielded zones would vary with Bingham number.

5.3. Effect of Bingham number on unyielded zones

The effect of Bingham number on the size and shape of the rigid zones is shown in Fig. 5. Similar to the trends seen for a circular

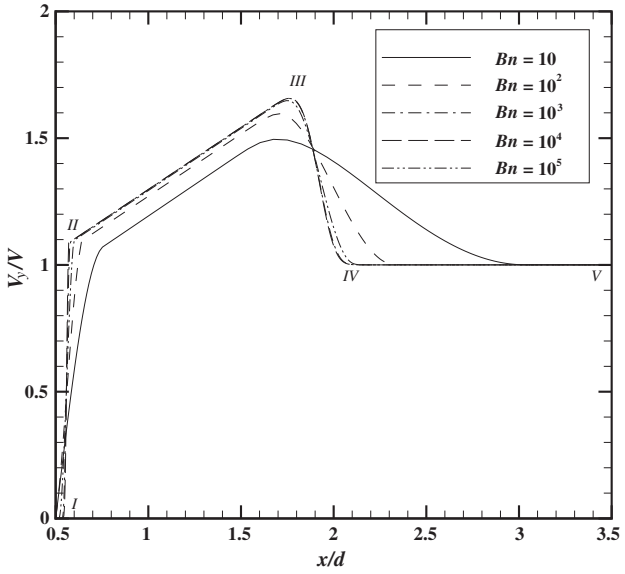

Fig. 9. Velocity profile along the line of symmetry($y = 0$) in the x-direction.

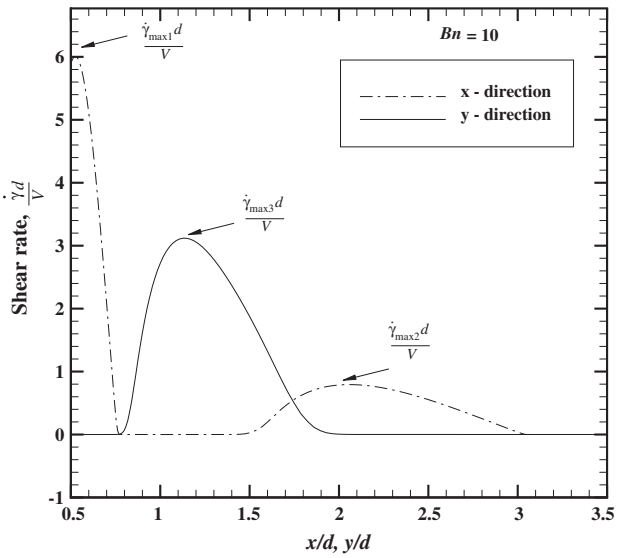

Fig. 11. Variation of shear rate along the line of symmetry in the x- and y-directions.

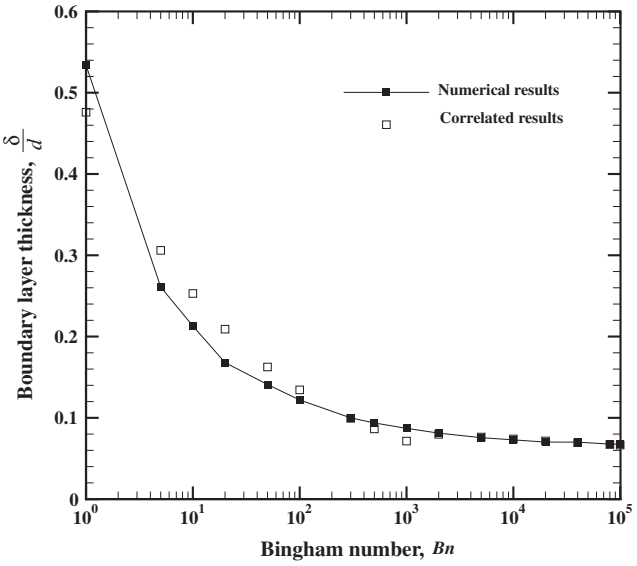

Fig. 10. Viscoplastic boundary layer thickness as a function of Bingham number.

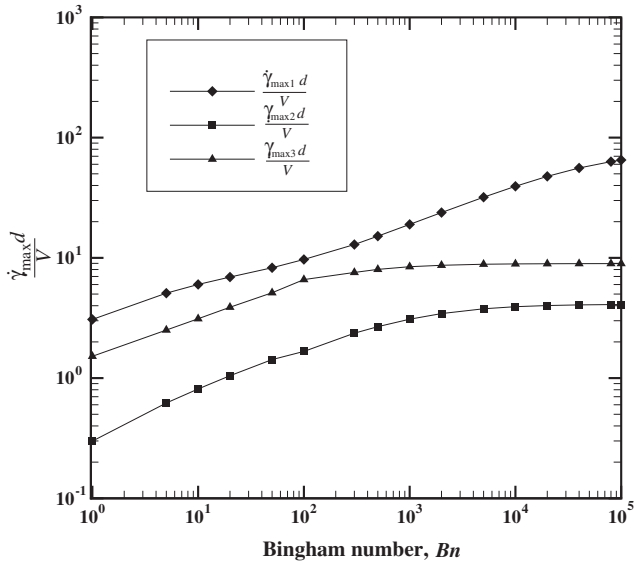

Fig. 12. Variation of $\frac{\dot{\gamma}_{max1}d}{V}$, $\frac{\dot{\gamma}_{max2}d}{V}$ and $\frac{\dot{\gamma}_{max3}d}{V}$ with Bingham number.

cylinder [21], the size of all rigid zones indicate Zr1, Zr2, Zr3 decreases with Bingham number, but beyond a certain Bingham number, it changes very little. The shaded regions in Fig. 5 show the unyielded zones. As expected, the size of the yield surface S1 decreases with the increasing Bingham number while that of the yield surfaces S2 and S3 increases thereby affirming the diminishing significance of viscous deformation induced by the flow. Included in this figure are also the predictions of the bi-viscosity model where the two results are seen to be in very good agreement with each other. We note here that the shape of the yield surfaces differ somewhat – mainly in the shape of the "islands" – from the kinematic failure mechanism (the "slip lines") assumed in the plasticity theory of Knappett et al. [35] (see Fig. 10 in [35]).

The change in the static zone, Zr2 is reported in Fig. 6. It is clear from Fig. 6 that on increasing the Bingham number, the size of the zone, Zr2 increases but at the same time the angle, ϕ decreases and becomes constant in the limit of large Bingham numbers, *i.e.*, $Bn \to \infty$. The same trend has been reported in the case of a circular cylinder [21]. At very high value of the Bingham number, the angle, becomes 90° which is the same as that predicted from the plasticity theory [35] and in the case of circular cylinders [21].

Fig. 6 shows the influence of the Bingham number on the dimensions of various rigid zones in both x- and y-directions. It is clear that the size of zone Zr3 increases slightly with the increasing Bingham number until $Bn \approx 10^3$ beyond which it essentially reaches the infinite Bingham number limit. In contrast, there is a significant decrease in the size of zone Zr3 in the x-direction with increasing Bingham number thereby making it thinner and thinner. The data also shows that with increasing Bingham number the size of zones Zr1 and Zr2 decreases in the y-direction while that of zone Zr3 increases. Finally, we have compared, Table 6, the relative dimensional characteristics of the rigid zones for circular and square cylinders at $Bn = 20$. The size of the rigid zones in both x and y-directions is always greater for a square cylinder than that for a circular cylinder. This may be due to the presence of the sharp corners in the case of a square cylinder.

5.4. Flow kinematics

Fig. 7 shows the sensitivity of the maximum (non-dimensional) shear rate at the surface of the cylinder to the grid used and the value of the growth rate parameter, m. Although the drag coefficient is essentially unaffected in this range of parameters over the whole range of Bingham number (see Table 2 for example), it is clear that the maximum value of shear rate is quite (∼10%) sensitive to the value of the growth rate parameter, especially at high Bingham number. Similarly, the shear rate is seen to be much more sensitive

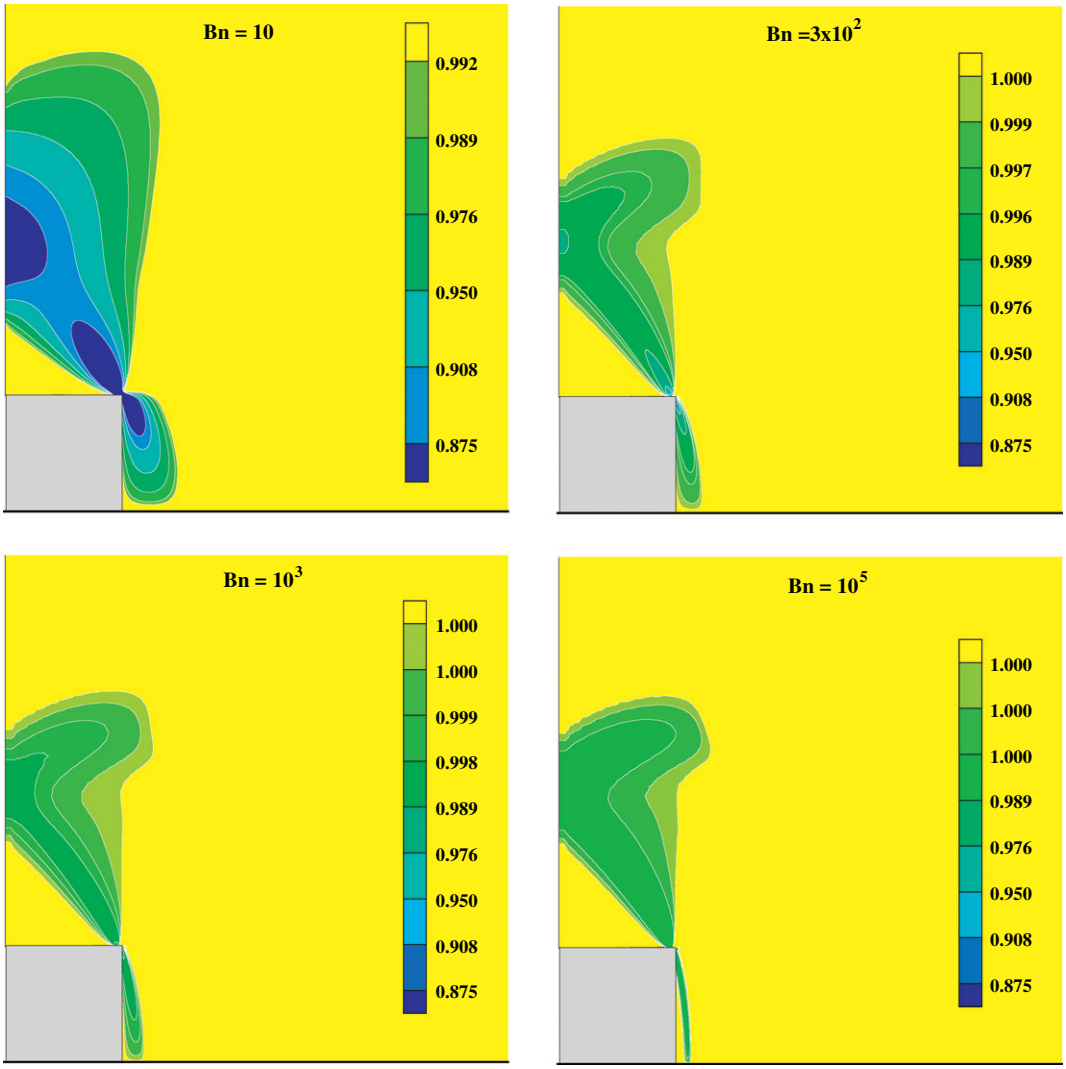

Fig. 13. Contours of normal stress, $\frac{\tau_{xx}}{\tau_0}$ in the vicinity of the cylinder.

to the choice of the solution grid thereby contributing to the degree of difficulty of such numerical studies.

Fig. 8 shows the velocity profile at the symmetry line in the y-direction (*i.e.* along line $x = 0$ in Fig. 1). The constant velocity in segments I–II and III–IV in Fig. 8 represents the rigid zones Zr2 and Zr1 respectively and the segment where the velocity is changing abruptly, segment III–IV, is nothing but the viscous fluid zone. It is also evident from Fig. 8 that zone Zr2 is a static zone and the zone Zr1 is a dynamic zone, moving with the plug velocity. These results show the profound influence of the Bingham number on the velocity profile up to about $Bn \leqslant \sim 10^3$ beyond which it becomes independent of Bingham number, thereby suggesting it to approach the limit of the fully plastic flow.

Fig 9 shows the velocity profile along the line of symmetry in the x-direction (*i.e.* along $y = 0$ in Fig. 1). Once again, there are four different deformation regions seen here; the first region; I–II, represents thin viscoplastic boundary layer fluid zone wherein very high shear rates cause abrupt change in the velocity profile. The region II–III represents the rigid zone, Zr3, which is, in fact, undergoing solid body rotation. The segment III–IV represents another fluid-like zone where the velocity is monotonically decreasing from point III to IV. Finally in the region, IV–V, the velocity profile becomes flat thereby suggesting a constant velocity, which represents the far-field rigid zone Zr1, moving as a solid plug. Here also, the Bingham number is seen to exert very little influence beyond $Bn > 10^3$.

Fig 10 shows the effect of Bingham number on the viscoplastic boundary layer thickness. The minimum thickness of the boundary layer has been calculated here by equating the velocity $V_y = 0.999V$ at the first point on line of symmetry in x-direction (*i.e.*, $\frac{\partial V_y}{\partial x} = 0$) from the surface of the cylinder. The variation of the boundary layer thickness with Bingham number is found to be qualitatively similar to that seen for a circular cylinder [21]. One can argue that the increasing Bingham number is equivalent to the increasing value of Reynolds number both of which lead to the progressive thinning of the momentum boundary layer. The present results can be well approximated by the following expressions:

$$\frac{\delta}{d} = 0.48Bn^{-0.27} \quad \text{for } 1 \leqslant Bn \leqslant 10^3 \tag{18a}$$

$$\frac{\delta}{d} = 0.11Bn^{-0.05} \quad \text{for } 2 \times 10^3 \leqslant Bn \leqslant 10^5 \tag{18b}$$

Eq. (18a) reproduces the present numerical results with an average error of 11.5% which arises to a maximum of 20% whereas the corresponding values for Eq. (18b) are less than 0.1%.

Fig 11 represents the magnitude of dimensionless strain rate tensor along the lines of symmetry in x- and y-directions at

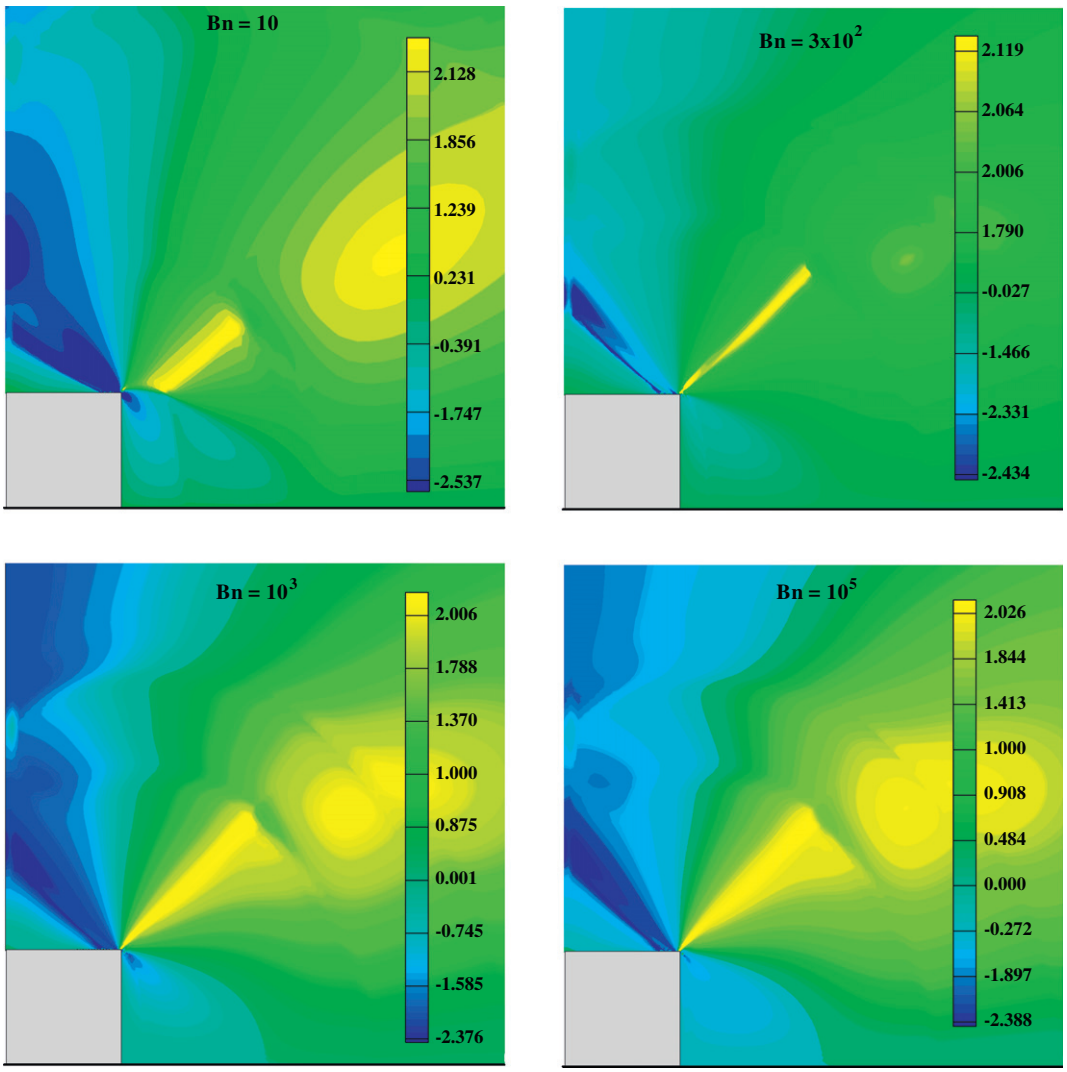

Fig. 14. Contours of normal stress difference, $\frac{\tau_{yy}-\tau_{xx}}{\tau_0}$ in the vicinity of the cylinder.

Bn = 10. There are two peaks on the first curve (broken line), one of these corresponds to the surface of the cylinder and the other one is situated in the fluid zone in between zones Zr1 and Zr3. This behaviour is also seen to be qualitatively similar to that for a circular cylinder [21]. The second curve (solid line) has only one maximum and it is seen to occur between zones Zr1 and Zr2. All three peak values increase with Bingham number, as shown in Fig 12.

5.5. Stress, velocity, pressure and shear rate fields on the surface of the cylinder

Figs. 13–15 show representative contours of various kinematic variables like stress, velocity, pressure and shear rate thereby giving an idea about the detailed structure of the flow on and/or near the surface of the square cylinder. Evidently, in the limit of low plastic effect, *i.e.*, small value of Bn, there is a significant variation in stresses in the vicinity of cylinder. On the other hand, in the limit of high plastic effects, there is an increasing density of contour lines near the cylinder thereby suggesting that the fluid-like zones shrink in size with the increasing value of the Bingham number, akin to thinning of the boundary layer. As $Bn \to \infty$ the contour lines of the normal stress approach the expected limiting behaviour, *i.e.*, $\frac{\tau_{xx}}{\tau_0} \to 1$, as also exhibited by the shear stress $\frac{\tau_{xy}}{\tau_0}$ (see Fig. 15). On the other hand, Fig. 14 shows the contours of normal stress difference $\frac{\tau_{yy}-\tau_{xx}}{\tau_0}$ and it is clear that in the limit of $Bn \to \infty$, it correctly approaches the expected limiting value of $\left|\frac{\tau_{yy}-\tau_{xx}}{\tau_0}\right| \to 2$. Fig. 16 depicts representative contours of the velocity, pressure and shear rate and as expected the slip line fields are seen to evolve slowly emerging in the limit of high Bingham number.

5.6. Drag coefficient

While the results presented in the preceding sections provide useful insights into the detailed structure of the flow and stress fields in the vicinity of the cylinder, reliable values of drag coefficient are frequently needed in process design calculations. For the present configuration and creeping flow regime, the drag coefficient is expected to be a function of the Bingham number only. Fig. 17 shows the dependence of the total and pressure drag coefficients on the Bingham number where both are seen to exhibit the classical inverse dependence on the Bingham number, which is also in line with that observed for a circular cylinder [21]. The dependence of the drag coefficient on Bingham number weakens for Bingham numbers above 10 ultimately becoming independent of Bn at about $Bn \geqslant 100$. The numerical data shown in Fig. 17 has been correlated using the non-linear regression analysis approach as follows (over the range $1 \leqslant Bn \leqslant 10^5$):

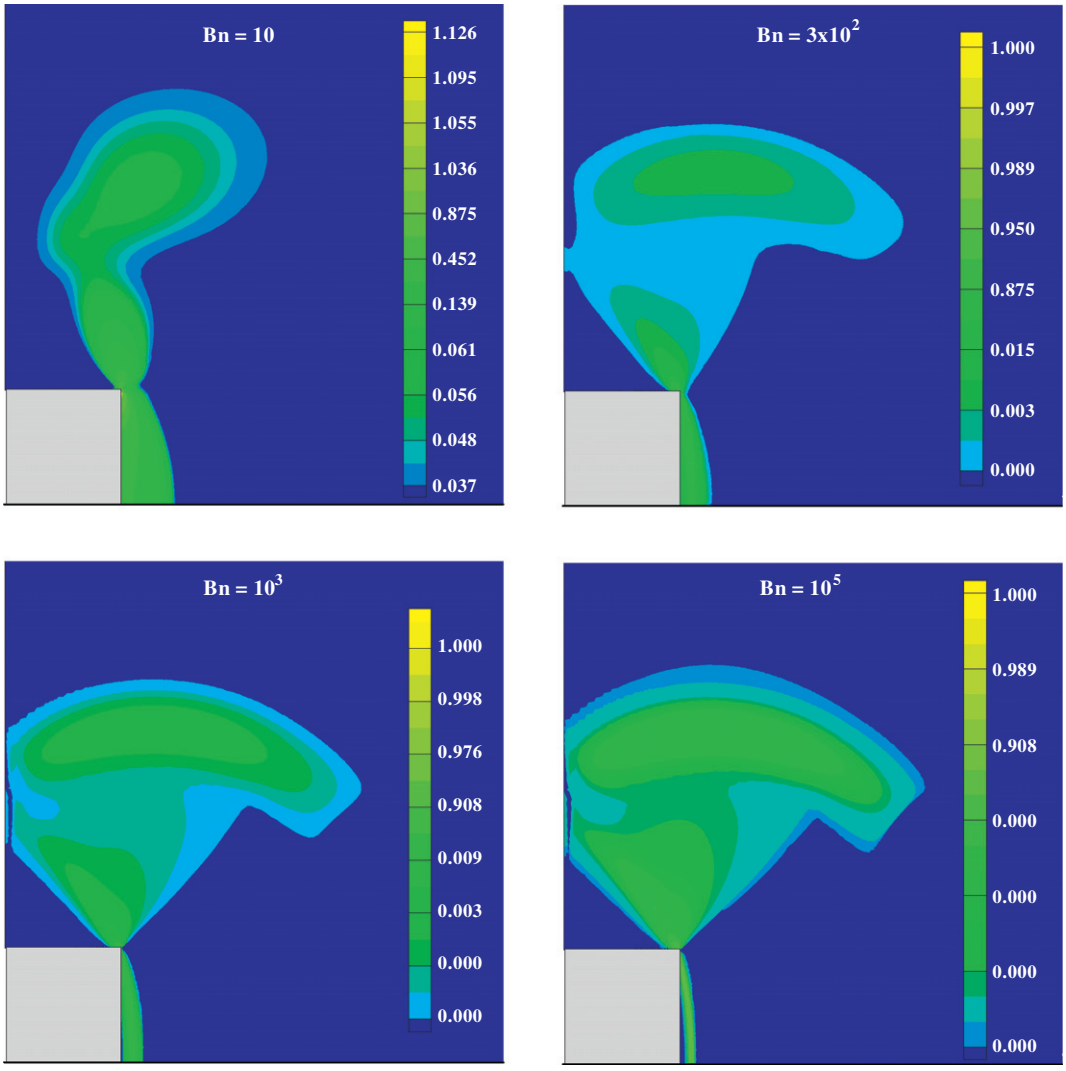

Fig. 15. Contours of shear stress, $\frac{\tau_{xy}}{\tau_0}$ in the vicinity of the cylinder.

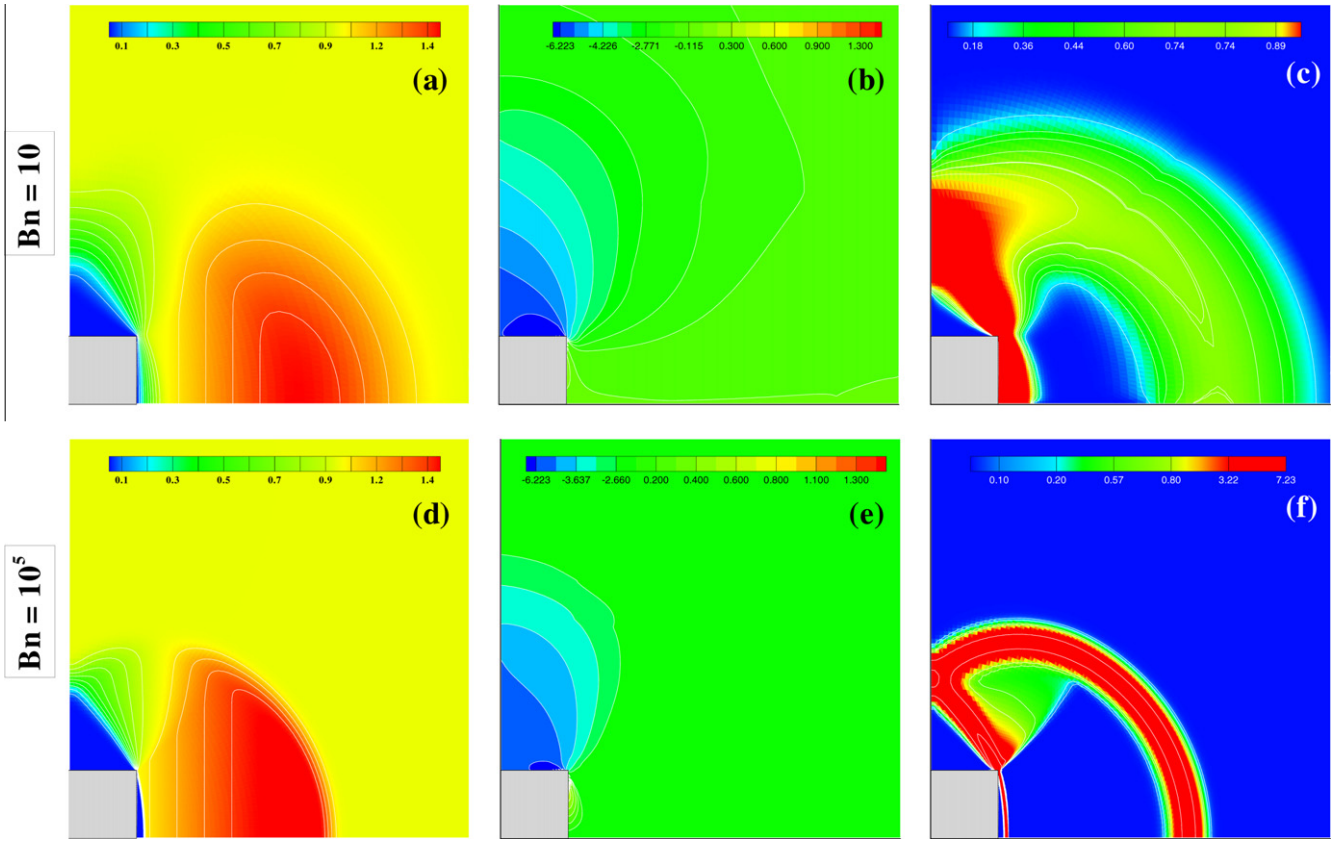

Fig. 16. Contours diagram: (a and d) velocity in *y*-direction, (b and e) pressure and (c and f) shear rate.

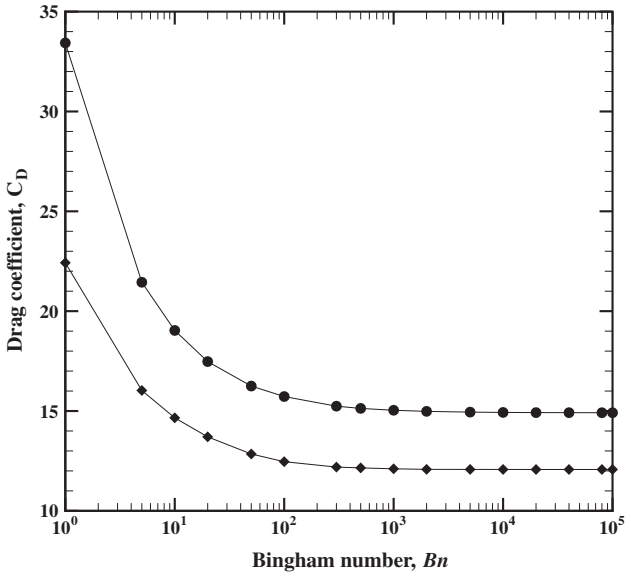

Fig. 17. Variation of drag coefficient (●) and pressure drag coefficient (♦) with Bingham number.

$$C_D = 14.91 + \frac{18.55}{Bn^{0.66}} \tag{19a}$$

$$C_{DP} = 12.07 + \frac{10.40}{Bn^{0.62}} \tag{19b}$$

Finally, to add further weight to our claim regarding the validity of the regularization scheme used here, computations have also been carried out by using the bi-viscosity model with $\mu_{yield} = 10^4\mu_B$,

Table 7
Values of drag coefficient for a square cylinder calculated by bi-viscosity model.

Bn	Papanastasiou model	Bi-viscosity model
1	33.43	33.42
10	19.02	19.02
10^2	15.72	15.71
10^3	15.04	15.03
10^4	14.92	14.96
10^5	14.91	14.92
10^6	14.91	14.92
10^7	14.91	14.92

similar to that used in [45] and the resulting values of the drag coefficient are summarized in Table 7 where the two results are seen to be virtually indistinguishable from each other. Such a close match inspires confidence in the use of the Papanastasiou regularization method at least as far as the drag calculations are concerned.

6. Conclusions

The creeping flow of a Bingham plastic fluid past a *2-D* square cylinder has been studied numerically using the finite element method. The inherent discontinuity in the original Bingham constitutive relation has been treated through the Papanastasiou regularization technique together with a growth rate parameter. The results based on this model have also been compared with that based on the bi-viscosity approach to ascertain their reliability. Finally, the results reported herein span five orders of magnitude variation in the value of Bingham number ($1 \leqslant Bn \leqslant 10^5$) and at $Bn = 10^5$, these are seen to approach their limiting values thereby becoming independent of the Bingham number. The detailed structure of the flow field is studied in terms of the spatial variation of

velocity and stress components which, in turn, help delineate the location, size and shape of the yield surfaces demarcating the so-called fluid (yielded) and solid (unyielded) like regions in the flow domain. Essentially, three types of unyielded regions are identified which are qualitatively similar (but larger) to that reported for a circular cylinder. As expected, all yielded regions shrink progressively with the increasing Bingham number. The utility of the notion of the viscoplastic boundary layer has also been demonstrated. In the limit of high Bingham number, the location of rigid zones and the value of drag coefficient is found to be constant and consistent with the predictions of bi-viscosity model.

Acknowledgements

We would like to thank the two anonymous reviewers for many critical and constructive comments on this work.

References

[1] R.B. Bird, G.C. Dai, B.J. Yarusso, The rheology and flow of viscoplastic materials, Rev. Chem. Eng. 1 (1983) 1–70.
[2] H.A. Barnes, Yield stress—a review or 'παντα ρ ε ι'—everything flows? J. Non-Newton. Fluid Mech. 81 (1999) 133–178.
[3] R.P. Chhabra, J.F. Richardson, Non-Newtonian Flow and Applied Rheology, second ed., Butterworth-Heinemann, Oxford, 2008.
[4] R.P. Chhabra, Bubbles, Drops and Particles in Non-Newtonian Fluids, second ed., CRC Press, Boca Raton, 2006.
[5] D.D. Atapattu, R.P. Chhabra, P.H.T. Uhlherr, Wall effect for sphere falling at small Reynolds number in a viscoplastic medium, J. Non-Newton. Fluid Mech. 38 (1990) 31–42.
[6] D.D. Atapattu, R.P. Chhabra, P.H.T. Uhlherr, Creeping motion in Herschel–Bulkley fluids: flow field and drag, J. Non-Newton. Fluid Mech. 59 (1995) 245–265.
[7] M. Hariharaputhiran, R.S. Subramanian, G.A. Campbell, R.P. Chhabra, The settling of spheres in a viscoplastic fluid, J. Non-Newton. Fluid Mech. 79 (1998) 87–97.
[8] H. Tabuteau, P. Coussot, J.R. de Bruyn, Drag force on sphere in steady motion through a yield stress fluid, J. Rheol. 51 (2007) 125–137.
[9] O. Merkak, L. Jossic, A. Magnin, Spheres and interactions between spheres moving at very low velocities in a yield stress fluid, J. Non-Newton. Fluid Mech. 133 (2006) 99–108.
[10] N.P. Chafe, J.R. de Bruyn, Drag and relaxation in a bentonite clay suspension, J. Non-Newton. Fluid Mech. 131 (2005) 44–52.
[11] T. Ferroir, H.T. Huynh, X. Chateau, P. Coussot, Motion of a solid object through a pasty (thixotropic) fluid, Phys. Fluids 16 (2004) 594–601.
[12] A.N. Beris, J.A. Tsamopoulos, R.C. Armstrong, R.A. Brown, Creeping motion of a sphere through a Bingham plastic, J. Fluid Mech. 158 (1985) 219–244.
[13] J. Blackery, E. Mitsoulis, Creeping motion of a sphere in tubes filled with a Bingham plastic material, J. Non-Newton. Fluid Mech. 70 (1997) 59–77.
[14] M. Beaulne, E. Mitsoulis, Creeping motion of a sphere in tubes filled with Herschel–Bulkley fluids, J. Non-Newton. Fluid Mech. 72 (1997) 55–71.
[15] M.M. Gumulya, R.R. Horsley, K.C. Wilson, V. Pareek, A new fluid model for particle settling in a viscoplastic fluid, Chem. Eng. Sci. 66 (2011) 729–739.
[16] B.T. Liu, S.J. Muller, M.M. Denn, Convergence of a regularisation method for creeping flow of a Bingham material about a rigid sphere, J. Non-Newton. Fluid Mech. 102 (2002) 179–191.
[17] T.C. Papanastasiou, Flow of materials with yield, J. Rheol. 31 (1987) 385–404.
[18] K. Adachi, N. Yoshioka, On creeping flow of a viscoplastic fluid past a circular cylinder, Chem. Eng. Sci. 28 (1973) 215–226.
[19] N. Roquet, P. Saramito, An adaptive finite element method for Bingham fluid flows around a cylinder, Comput. Meth. Appl. Mech. Eng. 192 (2003) 3317–3341.
[20] E. Mitsoulis, On creeping drag flow of a viscoplastic fluid past a circular cylinder: wall effects, Chem. Eng. Sci. 59 (2004) 789–800.
[21] D.L. Tokpavi, A. Magnin, P. Jay, Very slow flow of Bingham viscoplastic flow around a circular cylinder, J. Non-Newton. Fluid Mech. 154 (2008) 65–76.
[22] B.D.D. Besses, A. Magnin, P. Jay, Viscoplastic flow around a cylinder in an infinite medium, J. Non-Newton. Fluid Mech. 115 (2003) 27–49.
[23] T. Zisis, E. Mitsoulis, Viscoplastic flow around a cylinder kept between parallel plates, J. Non-Newton. Fluid Mech. 105 (2002) 1–20.
[24] S. Mossaz, P. Jay, A. Magnin, Criteria for the appearance of recirculating and non-stationary regimes behind a cylinder in a viscoplastic fluid, J. Non-Newton. Fluid Mech. 165 (2010) 1525–1535.
[25] P. Sivakumar, R.P. Bharti, R.P. Chhabra, Effect of power-law index on critical parameters for a power-law flow across an unconfined circular cylinder, Chem. Eng. Sci. 61 (2006) 6035–6046.
[26] A. Putz, I.A. Frigaard, Creeping flow around particles in a Bingham fluid, J. Non-Newton. Fluid Mech. 165 (2010) 263–280.
[27] I. Frigaard, C. Nouar, On the usage of viscosity regularisation methods for visco-plastic fluid flow computation, J. Non-Newton. Fluid Mech. 127 (2005) 1–26.
[28] M. Bercovier, M. Engelman, A finite element method for incompressible non-Newtonian flows, J. Comput. Phys. 36 (1980) 313–326.
[29] B.T. Liu, S.J. Muller, M.M. Denn, Interactions of two rigid spheres translating collinearly in creeping flow in a Bingham material, J. Non-Newton. Fluid Mech. 113 (2003) 49–67.
[30] D.L. Tokpavi, P. Jay, A. Magnin, Interaction between two circular cylinders in slow flow of Bingham viscoplastic fluid, J. Non-Newton. Fluid Mech. 157 (2009) 175–187.
[31] L. Jossic, A. Magnin, Drag of an isolated cylinder and interactions between two cylinders in yield stress fluids, J. Non-Newton. Fluid Mech. 164 (2009) 9–16.
[32] J.G. Oldroyd, 2D plastic flow of a Bingham solid—a plastic boundary layer theory for slow motion, Proc. Cambridge Philos. Soc. 43 (1947) 383–395.
[33] J.M. Piau, Viscoplastic boundary layer, J. Non-Newton. Fluid Mech. 102 (2002) 193–218.
[34] M.F. Randolph, G.T. Houlsby, The limiting pressure on a circular pile loaded laterally in cohesive soil, Geotechnique 34 (1984) 613–623.
[35] J.A. Knappett, S. Mohammadi, C. Griffin, Lateral spreading forces on bridge piers and pile caps in laterally spreading soil: effect of angle of incidence, J. Geotech. Geoenviron. 136 (2010) 1589–1599.
[36] C.M. Martin, M.F. Randolph, Upper-bound analysis of lateral pile capacity in cohesive soil, Geotechnique 56 (2006) 141–145.
[37] F. Savreux, P. Jay, A. Magnin, Flow normal to a flat plate of a viscoplastic fluid with inertial effects, AIChE J. 51 (2005) 750–758.
[38] C. Atkinson, K. El-Ali, Some boundary value problems for the Bingham model, J. Non-Newton. Fluid Mech. 41 (1992) 339–363.
[39] R.V. Craster, Solutions for Herschel–Bulkley flows, Quart. J. Appl. Math. 48 (1995) 343–374.
[40] K. El-Ali, C. Atkinson, Boundary value problems involving Herschel–Bulkley material, IMA J. Appl. Math. 51 (1993) 169–186.
[41] R.V. Craster, C. Atkinson, Yield surfaces for Herschel–Bulkley flows in complex geometries, IMA J. Appl. Math. 56 (1996) 253–276.
[42] A. Sharma, V. Eswaran, Heat and fluid flow across a square cylinder in two-dimensional laminar flow regime, Numer. Heat Trans. A 45 (2004) 247–269.
[43] A.K. Dhiman, R.P. Chhabra, V. Eswaran, Steady flow of power-law fluid across a square cylinder, Chem. Eng. Res. Des. 84 (2006) 300–310.
[44] P. J. Roache, Fundamentals of Computational Fluid Dynamics, Hermosa, Albuquerque, NM, 1998.
[45] O. Turan, R.J. Poole, N. Chakraborty, Aspect ratio effects in laminar natural convection of Bingham fluids in rectangular enclosures with differentially heated side walls, J. Non-Newton. Fluid Mech. 166 (2011) 208–230.